iScience

CellPress

Article

Real-Time *In Vivo* Control of Neural Membrane Potential by Electro-Ionic Modulation

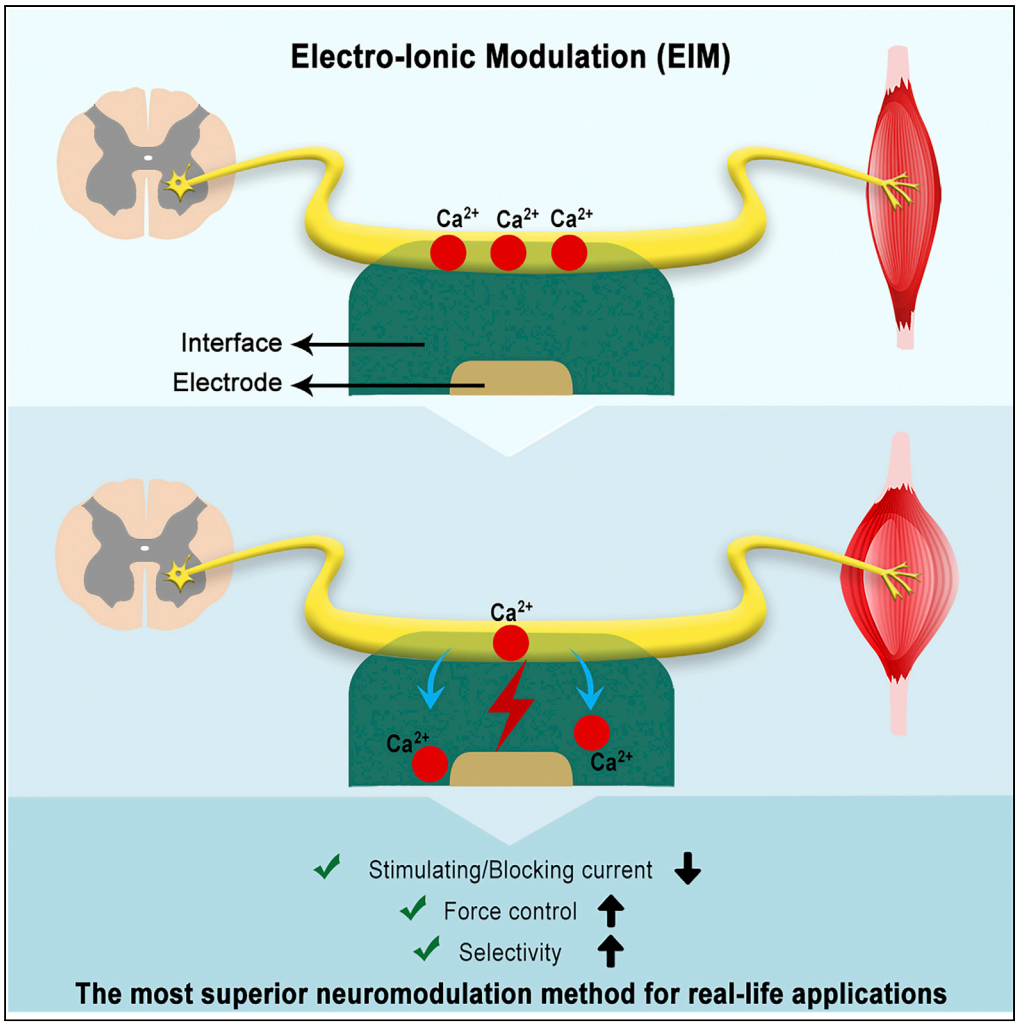

Zafer Soybaş, Sefa Şimşek, F.M. Betül Erol, ..., Bahattin Aydoğdu, Çağlar Elbüken, Rohat Melik

rmelik@etu.edu.tr

HIGHLIGHTS

EIM regulates extracellular ion concentration *in vivo* in real time

EIM stimulates or blocks the nerve via Ca^{2+} ion depletion or enhancement

EIM achieves selective stimulation or blocking of large or small axons

EIM is the most superior neuromodulation method for real-life applications

Soybaş et al., iScience *17*, 347–358
July 26, 2019
https://doi.org/10.1016/j.isci.2019.06.038

iScience

CellPress

Article

Real-Time *In Vivo* Control of Neural Membrane Potential by Electro-Ionic Modulation

Zafer Soybaş,[1,5] Sefa Şimşek,[1,5] F.M. Betül Erol,[2] U. Çiya Erdoğan,[1] Esra N. Şimşek,[1] Büşra Şahin,[1] Merve Marçalı,[3] Bahattin Aydoğdu,[4] Çağlar Elbüken,[3] and Rohat Melik[1,6,*]

SUMMARY

Theoretically, by controlling neural membrane potential (V_m) *in vivo*, motion, sensation, and behavior can be controlled. Until now, there was no available technique that can increase or decrease ion concentration *in vivo* in real time to change neural membrane potential. We introduce a method that we coin *electro-ionic modulation* (EIM), wherein ionic concentration around a nerve can be controlled in real time and *in vivo*. We used an interface to regulate the Ca^{2+} ion concentration around the sciatic nerve of a frog and thus achieved stimulation and blocking with higher resolution and lower current compared with electrical stimulation. As EIM achieves higher controllability of V_m, it has potential to replace conventional methods used for the treatment of neurological disorders and may bring a new perspective to neuromodulation techniques.

INTRODUCTION

During the evolutionary process, the neuromuscular system, which functions through the V_m change, is developed to make the organisms able to sense and move (Weiss, 1996; Campbell et al., 2015; Butler and Hodos, 2005). Therefore, in theory, if we manage to control V_m *in vivo*, we can control motion and sensation (Weiss, 1996). To control V_m, there are four known parameters that can be regulated: pH, temperature, extracellular ion concentration, and application of extrinsic current (Weiss, 1996). In literature, techniques that change only one of these parameters were generally used (Ho et al., 2014; Harris, 2008). For instance, functional electrical stimulation (FES) uses electrical stimulation method. FES has several clinical applications for restoring the neurological functions in paralyzed patients such as control of upper extremity (Memberg et al., 2014; Micera et al., 2010; Hochberg et al., 2012; Bouton et al., 2016; Peckham and Kilgore, 2013), lower extremity (Rohde et al., 2012; Triolo et al., 2012; Nataraj et al., 2012; Sadowsky et al., 2013), respiratory muscles (Elefteriades et al., 2002; Onders et al., 2004), posture (Wu et al., 2013; Triolo et al., 2013a, 2013b), gait (Wenger et al., 2016; Mazurek et al., 2012), and prevention of pressure ulcers (Solis et al., 2011, 2012). However, because the stimulation current used in FES is too high, it may cause over-heating in tissues, leading to nerve damage (Ho et al., 2014). Also, because it cannot selectively stimulate or block the nerves, localization of signal propagation cannot be achieved. As a result, it activates the related sensory nerve fibers resulting in pain sensation (Peckham and Knutson, 2005). Another reason FES has a limited use in daily life is that nerve blockage cannot be achieved in a controlled manner (Peckham and Knutson, 2005). In addition, there are some direct clinical applications for blocking such as regaining of bladder control in neurologically disabled patients (Boger et al., 2012).

Another major approach to change V_m is using chemical methods to change ion concentration. Some pharmacological agents are used for this purpose. For example opiates, such as morphine and codeine, are commonly used in pain management (Kandel et al., 2013). However, they can lead to systemic side effects such as nausea, constipation, urinary retention, respiratory depression, and cardiac arrest (Peckham and Knutson, 2005; Kandel et al., 2013; Choi, 2016). These adverse effects cause patients to discontinue the medication (Gilron et al., 2015). To establish more control over V_m, extracellular ion concentration was changed and extrinsic current was applied, but there is no available technique that can simultaneously combine them. Electrochemical methods (van den Brand et al., 2012), in which extrinsic current stimulates the nerve after injecting some chemicals, are developed for controlling V_m. However, as they use the injection method for changing chemical concentration, they can only alter the neural membrane environment once, hence lacking the real-time modulation ability. Previously, *in vitro* ion concentration was changed

[1]Department of Electrical and Electronics Engineering, TOBB University of Economics & Technology, Ankara 06510, Turkey

[2]Faculty of Medicine, Hacettepe University, Ankara 06100, Turkey

[3]Institute of Materials Science and Nanotechnology, National Nanotechnology Research Center (UNAM), Bilkent University, Ankara 06800, Turkey

[4]Department of Pediatric Surgery, Dicle University Medical Faculty, Diyarbakır 21280, Turkey

[5]These authors contributed equally

[6]Lead Contact

*Correspondence: rmelik@etu.edu.tr

https://doi.org/10.1016/j.isci.2019.06.038

by ion-selective membrane (ISM) (Song et al., 2011). This study first changes the neural membrane environment and then electrically stimulates the nerve; hence it changes ion concentration and applies current separately, which causes delay. Because of this one-minute-delay (Luan et al., 2014; Theogarajan, 2012) this method is not suitable for use in real-life applications such as prosthesis for motion and retina (Theogarajan, 2012). Another method targeting to control V_m is optogenetics (Boyden et al., 2005). This technique aims to change ion concentration around the nerve via light. To achieve this, optogenetics genetically modifies the neurons to make them sensitive to light. However, optogenetics is not suitable for daily-life applications and can only be used for research purposes because it genetically alters the neurons for modifying ion channels. In sum, until now there has been no technique that can change V_m *in vivo* in real time with high control and be applicable to real life. We have developed a method, electro-ionic modulation (EIM) that achieves neuromodulation via real-time regulation of extracellular ion concentration around the nerve *in vivo* and application of extrinsic current to the nerve at the same time by using an electrode and an interface on it. In this work we used ISM as the interface to change ion concentration, but any other interface can be used for the purpose of EIM such as uniform films, nanoparticles, peptides, or polymers. EIM would enable better regulation of V_m compared with the traditional approaches, which have high potential to affect a variety of neuromodolution applications.

RESULTS

We first aimed to decrease the current needed for stimulation, and thus reduced power consumption and prevented nerve damage with EIM by using flexible electrodes coated with ISM. The fabrication procedure for flexible electrodes and ISM coating can be seen in the Transparent Methods section. As shown in Figure S1, we obtained the lowest threshold value with the flexible electrode compared with conventional cable method and the planar electrode, because flexible electrode increases the contact area between the nerve and the electrode surface. Therefore, we stimulated the nerve by using flexible electrode through all experiments.

EIM with Ca^{2+} Ion Depletion

We coated the flexible electrode with ISM for changing ion concentration around the nerve to obtain more excitable membrane environment. In literature, ISM is generally used in sensors to obtain selectivity (Gao et al., 2016; Plesha et al., 2006); however, we utilized ISM to actively change the neural membrane environment. To observe the effects of ion concentrations on nerve stimulation, we made separate *in vivo* manual ion injection experiments of PO_4^{3-}, Ca^{2+}, Na^+, and K^+ ions in the sciatic nerve of frogs. We used PO_4^{3-} ion to observe the effect of the Ca^{2+} ion depletion. The manual ion injection procedures can be seen in the Transparent Methods section. The threshold values before and after the ion injection are summarized in Figure S2. We obtained the most efficient results with PO_4^{3-}. Thus, we conclude that Ca^{2+} has a high impact on threshold regulation for nerve stimulation; hence we focused on changing the Ca^{2+} concentration.

The Ca^{2+} ion is critical for stimulation because it blocks the voltage-gated Na^+ channels (Armstrong and Cota, 1999). Therefore, depletion of Ca^{2+} ions around the nerve makes the stimulation easier because opening voltage-gated Na^+ channels facilitates the nerve stimulation (Kandel et al., 2013). The mechanism for the effect of Ca^{2+} ion on nerve stimulation is shown in Figure S3. Hence, we can conclude that the stimulation of nerve is easier with Ca^{2+} ion depletion around the nerve.

Stimulation Experiments with Ca^{2+} Ion Depletion

After exploring the effectiveness of the Ca^{2+} ion, we made *in vivo* EIM nerve stimulation experiments using flexible electrodes coated with ISM. In this section, we examined the nerve stimulation using EIM, which we coined *electro-ionic stimulation* (EIS). We compared the results of EIS and electrical stimulation in this section. Figure 1A (top) shows the experimental setup used for both stimulation and blocking experiments. Figure 1A (bottom) demonstrates the folded flexible electrodes used in stimulation and blocking experiments. As we applied enough force to fold our flexible electrodes, we did not use anything to hold the electrodes in folded state. Once the flexible electrodes are folded, they are held in folded state for days. We started the experiments by anesthetizing the frog. Details of anesthesia and frog preparation procedures are given in the Transparent Methods section. Subsequently, we stimulated the sciatic nerve of the frog *in vivo* with the stimulating electrode by pulsed DC signal applied from the function generator, as can be seen in Figure 1A (top). When the sciatic nerve was stimulated, the gastrocnemius muscle contracted and we measured the contractile force with the force transducer. Figure 1B (left) demonstrates the schematic drawing

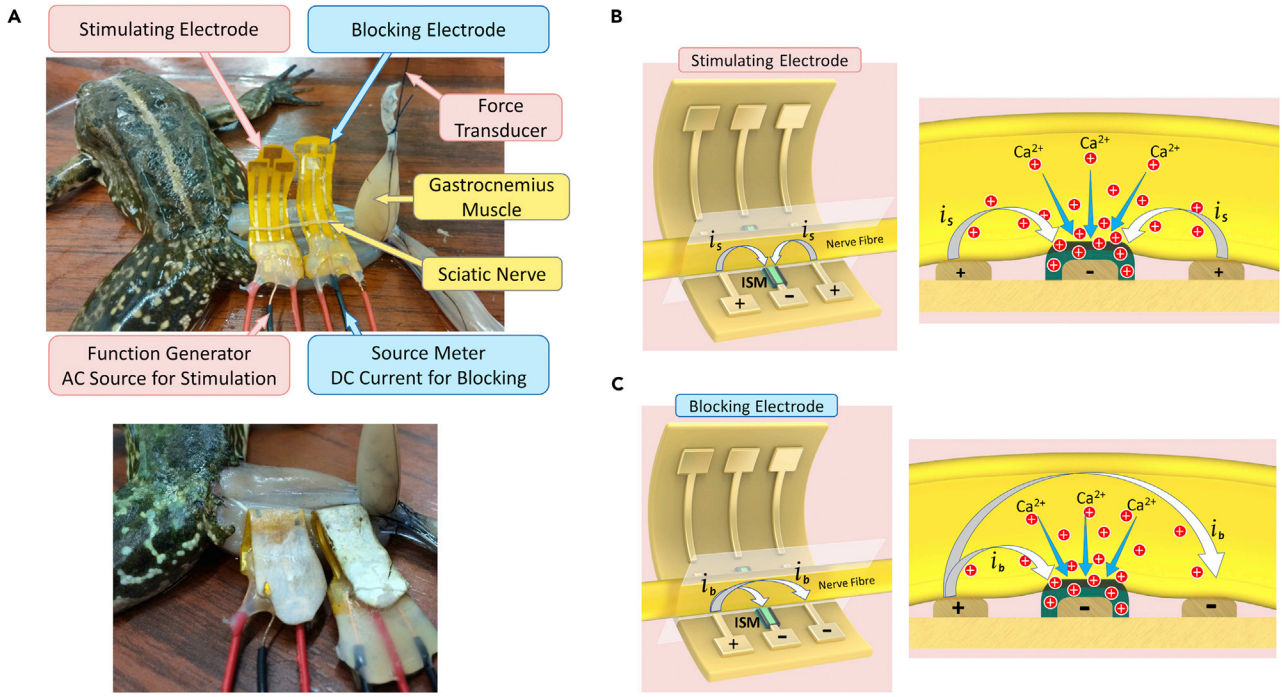

Figure 1. Experimental Setup and Operating Principle of Electro-ionic Modulation with Ca^{2+} Ion Depletion

(A) Photograph of the *in vivo* EIM stimulation and blocking experiments (top) and of the folded flexible electrodes used in *in vivo* EIM stimulation and blocking experiments (bottom).

(B) Schematic drawing of the flexible stimulating electrode and the operating principle of the device (left); cross section of sciatic nerve and flexible stimulating electrode to demonstrate the operating principle of ion-selective membrane (ISM) (right).

(C) Schematic drawing of the flexible blocking electrode and the operating principle of the device (left); cross section of sciatic nerve and flexible blocking electrode to demonstrate the operating principle of ISM (right).

of the flexible electrode and illustrates the operating principle of the device. The electrode is polarized as (+/-/+) configuration, and ISM is coated on the negatively polarized middle pole. The stimulating current flows from positively polarized poles to negatively polarized pole, and the nerve is stimulated through the negative pole. As can be observed in the cross-sectional view of the sciatic nerve and flexible stimulating electrode shown in Figure 1B (right), the negatively polarized ISM attracts the positively charged Ca^{2+} ions from the nerve thereby depleting Ca^{2+} ions around the nerve. As a result, we obtained a more excitable membrane environment and increased the V_m and hence decreased the threshold for stimulation.

In our experiments, we applied an input pulse from the function generator and measured the output force using the force transducer. We first stimulated the sciatic nerve with bare side of the electrode and recorded the stimulation threshold. Then we put the nerve onto the ISM-coated side of the electrode and recorded the threshold for a comparative analysis. We accepted the recorded voltage as the threshold value, when at least 80% of the applied pulses induce muscle contraction. The results of stimulation experiments are summarized in Figure 2. As can be seen in Figure 2A, the stimulation threshold decreases from 84 to 68 mV on the ISM-coated electrode. We got an average decrease of 22% in the threshold for three experiments. In our experiments, we obtained stimulation threshold ranging from 68 to 90 mV using ISM and obtained 39% energy saving; however, in the literature, 10% energy saving was achieved by optimizing the electrical stimulator circuit in rat's sciatic nerve (Foutz et al., 2012).

For validation of the working principle, we prepared a control experiment to prove that the decrement in the threshold is due to Ca^{2+} ion depletion around the nerve. For this experiment, we used polyvinyl chloride (PVC) membrane, which has the same content as ISM except for the Ca^{2+} ionophore, which is the part responsible for Ca^{2+} ion depletion (Wang et al., 2001; Kang and Hilgemann, 2004). When we compare the results given in Figure 2B, the threshold values in the bare electrode and the PVC-coated electrode are very similar, whereas there is a significant decrease with ISM-coated electrode. Hence we conclude

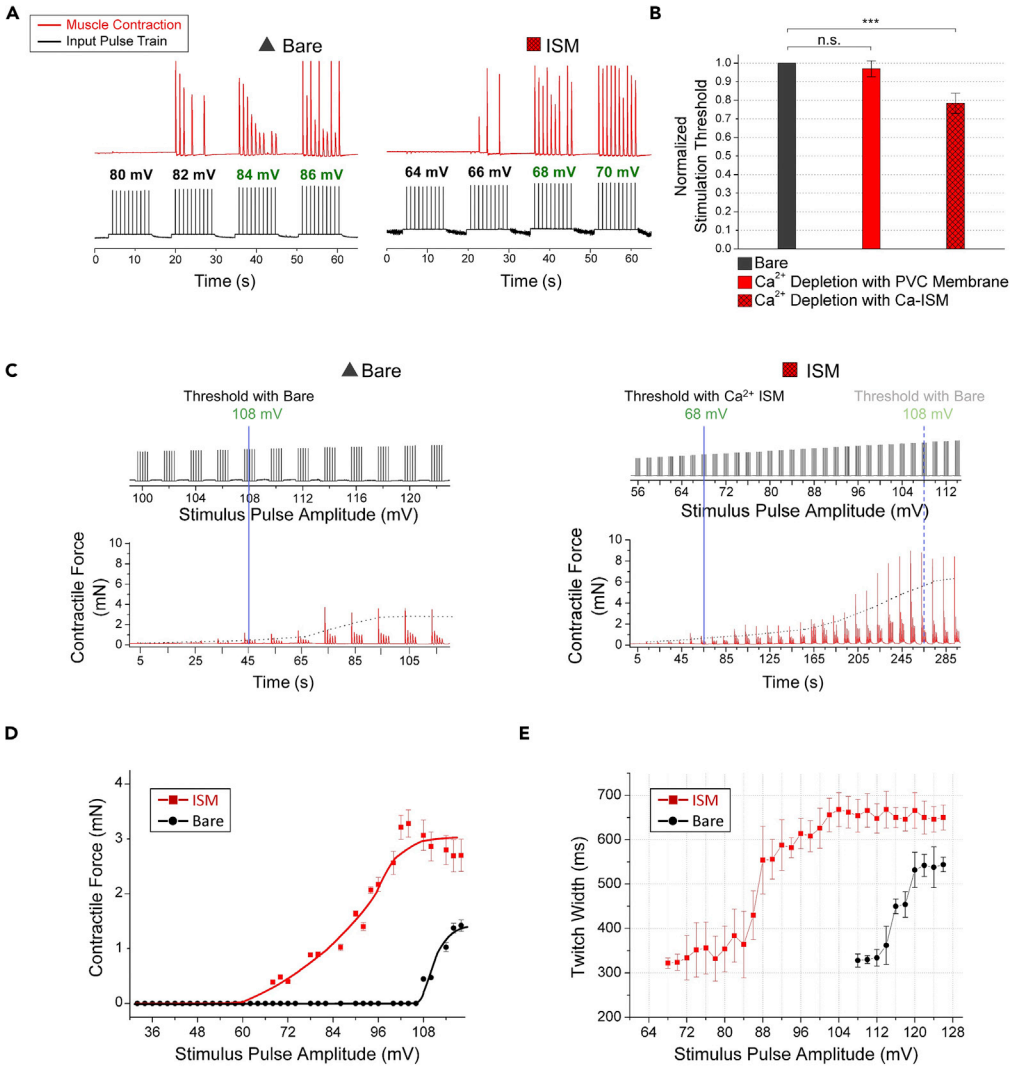

Figure 2. Results of Stimulation Experiments with Ca^{2+} Ion Depletion

(A) Stimulation experiment results for bare electrode and ISM-coated electrode. The stimulation threshold decreases from 84 to 68 mV on the ISM-coated electrode.

(B) Comparison of stimulation threshold values for bare electrode, PVC-coated electrode, and ISM-coated electrode (n = 3). The values are normalized with respect to bare electrode. The threshold values for the bare electrode and the PVC-coated electrode are very similar, whereas there is 22% decrement with ISM-coated electrode. V_s = 10 mV→110 mV in 2-mV step (stimulus), t_p = 1 ms (pulse width), f = 1 Hz (pulse frequency), n.s., not significant, ***p < 0.001, error bars represent 2 SD.

(C) Contractile force (mN) obtained for varying stimulus pulse amplitude (mV) for the bare electrode (left) and ISM-coated electrode (right). Higher dynamic range (higher maximum contractile force) is attained with ISM-coated electrode.

(D) Average and standard deviation of contractile force (mN) measured for varying stimulus pulse amplitude (mV) for the bare electrode and ISM-coated electrode obtained from the results in (C). Better resolution is acquired with ISM-coated electrode.

(E) Average and standard deviation of contractile force twitch width (ms) measured for varying stimulus pulse amplitude (mV) for bare electrode and ISM-coated electrode obtained from the results in (C). First large and then small axons are stimulated with ISM-coated electrode.

that the reduction in the stimulation threshold using ISM-coated electrode originates from the Ca^{2+} ion depletion around the nerve.

We performed control experiments for Ca^{2+} ion modulation using ISM in Figure S4. First, we performed Ca^{2+} imaging experiments as additional control experiments to prove Ca^{2+} ion attraction via ISM. The schematic

diagram of our experimental setup is given in Figure S4A. Using our planar electrodes coated with ISM, we applied 10 μA current for 65 s. The negatively charged ISM attracts positively charged Ca^{2+} ions. As a result, Ca^{2+} ions bind with Fluo-4 AM dye and Fluo-4 AM emission is increased as depicted in Figure S4B. The Fluo-4 AM fluorescence intensity is also increased as demonstrated in Figure S4D (left). We also calculated the Ca^{2+} ion concentration increase using the measured fluorescence intensity. The Ca^{2+} ion concentration after 10 μA current application for 5 s was 73.65 nM; however, Ca^{2+} ion concentration after 10 μA current application for 65 s was 715 nM. This experiment proves that we attracted Ca^{2+} ions using ISM. The Ca^{2+} imaging procedure and the details of Ca^{2+} ion concentration calculation can be seen in Transparent Methods section. The Ca^{2+} ion attraction experiment results are demonstrated in Video S1. In addition to the Ca^{2+} imaging experiments, we performed confocal imaging experiments of the sciatic nerve of a frog to prove the depletion of Ca^{2+} ions from the nerve using our device. Figure S4E demonstrates the results of the confocal imaging experiment. Figure S4E (left) exhibits the confocal imaging of the sciatic nerve before current application. Figure S4E (right) depicts another confocal image of the sciatic nerve after 20 μA current application for a minute. Because the negatively charged ISM attracts positively charged Ca^{2+} ions from the sciatic nerve after current application, we observe decrease in the fluorescence intensity of the Fluo-4 AM (Ca^{2+} reporter dye) in the sciatic nerve in Figure S4E (right). Therefore, Ca^{2+} ions were depleted from the sciatic nerve. This experiment demonstrates that we depleted Ca^{2+} ions from sciatic nerve of a frog using ISM. The details of the confocal imaging techniques can be seen in the Transparent Methods section.

We also performed experiments to test the Ca^{2+} ion selectivity of our device in Figure S5. We measured the resistance of our test setup using different concentrations of Ca^{2+} solution in Figure S5A. We obtained lowest resistance value with highest Ca^{2+} concentration and highest resistance value with lowest Ca^{2+} concentration as demonstrated in Figure S5C. These results show the Ca^{2+} ion selectivity of our device. We also performed additional control experiments with different concentrations of NaCl solution using the same ISM (Figure S5B). As Ca^{2+} ions pass much more than Na^{+} ions through Ca^{2+} ISM (Wang et al., 2001), we measured much higher resistances with NaCl solutions as depicted in Figure S5C. These results validate the Ca^{2+} ion selectivity of our device. The details of Ca^{2+} ion selectivity experiments can be seen in the Transparent Methods section.

After decreasing the threshold for stimulation, we performed experiments to evaluate the control on stimulation using ISM. For this purpose, we first observed the maximum magnitude of the contractile force, which we define as dynamic range. As shown in Figure 2C, we increased the maximum contractile force with ISM-coated electrode in addition to decreasing the threshold. The underlying mechanism of dynamic range increase is the selective stimulation of axons. As large axons have lower resistance, they are stimulated more easily than small axons (Kandel et al., 2013). Because we decrease the threshold, we can stimulate both large and small axons with the ISM-coated electrode, whereas only large axons can be stimulated in bare electrode case. As higher number of axons are stimulated using ISM, we obtain higher contractile force and hence higher dynamic range. When dynamic range increases, stronger movements can be achieved, which can be helpful to improve the performance of neuroprostheses such as the ones used in correcting foot drop (Melo et al., 2015).

In addition to obtaining a higher dynamic range, we also achieved better resolution, which we define as the inverse of the slope of the contractile force over the stimulus amplitude, with ISM-coated electrode. Resolution is calculated as 7.35 mV/mN for bare electrode and 17.88 mV/mN for ISM-coated electrode from the results shown in Figure 2D. The rationale behind this increase in resolution is also related to stimulation of first large and then small axons with the ISM-coated electrode. At 60 mV, we stimulate large axons with ISM-coated electrode; however, no stimulation is observed in bare electrode. Around 108 mV, small axons are stimulated by ISM-coated electrode, whereas for bare electrode, threshold is just achieved and only large axons start to be stimulated. Besides, contractile force saturates nearly at the same stimulus for ISM-coated electrode and bare electrode. Therefore, we stimulate axons in a wider range of stimulus with ISM and hence acquire better resolution, which enables us to have better control over the nerve stimulation. Better resolution is important especially in terms of achieving fine motor skills, such as movement of fingers.

We can deduce that we first stimulate the large axons and then small axons with ISM-coated electrode by exploring the relation between the input pulse and the twitch width of the gastrocnemius muscle. It is known that the velocity of the signal propagation is proportional to the square root of the axon diameter (Weiss, 1996). Furthermore, as signal propagation along the axon gets slower, higher twitch width is obtained (Ridge, 1967). As can be seen in Figure 2E, when we stimulate the nerve with ISM-coated

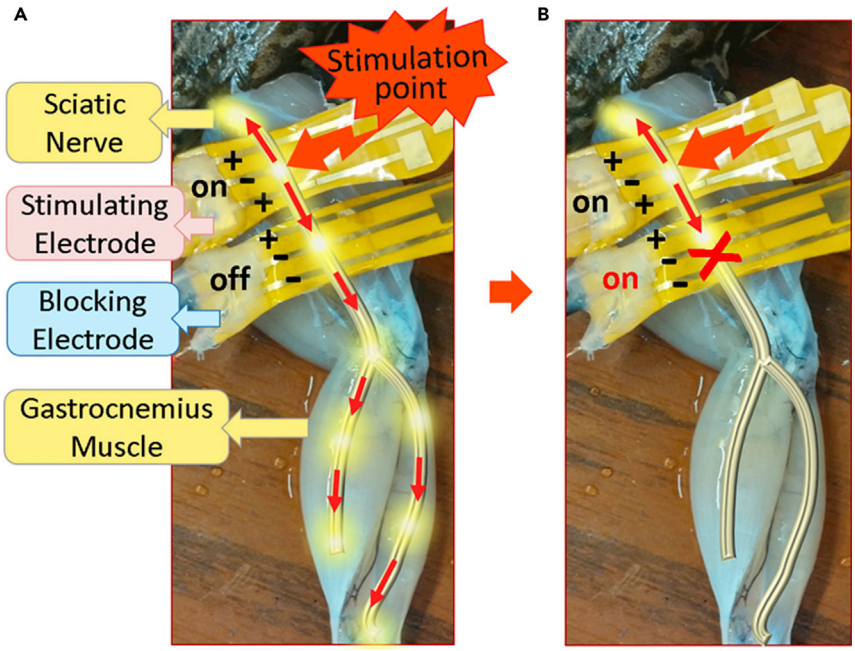

Figure 3. The Working Principle of Our Blocking Method

(A) When the stimulation current is applied and the blocking electrode is off, the signal propagates bidirectionally.

(B) When blocking electrode is turned on, the signal stops to propagate downward as depicted in right.

electrode, we first obtain low twitch width, which means that we first stimulate large axons. Then as we increase the input pulse, the twitch width increases, implying that we stimulate the small axons. This observation proves that we first stimulate large and then small axons with ISM-coated electrode.

Blocking Experiments with Ca^{2+} Ion Depletion

Following the selective stimulation with decreased stimulation threshold using ISM-coated electrode, we worked on blocking experiments and aimed to achieve controlled blocking with EIM. Figure 3 depicts the working principle of our blocking method. When the stimulation is applied and the blocking electrode is off, the signal propagates bidirectionally. When we turn on the blocking electrode, the signal stops to propagate downward. The signal cannot reach gastrocnemius muscle and contractions are terminated, hence we manage to localize the stimulation.

We again make use of the flexible electrodes coated with ISM to control blocking of the nerves. We performed blocking experiments with conventional cable method, planar electrode, and flexible electrode. Unsurprisingly, we obtained the lowest blocking current values with flexible electrodes as a consequence of increased contact area, as shown in Figure S6.

In addition to using flexible electrodes, we utilized ISM and depleted Ca^{2+} ions around the nerve to facilitate blocking through DC current application. Pulsed DC current is applied for stimulation, whereas DC current is applied for blocking because inactivation gate of voltage-gated Na^{+} channels is closed with prolonged current application (Kandel et al., 2013). Na^{+} channels should be in open position to go into inactivation phase (Kandel et al., 2013). Moreover, Ca^{2+} ion blocks the voltage-gated Na^{+} channels (Armstrong and Cota, 1999). Therefore, depletion of Ca^{2+} ions around the nerve with DC current application makes the blocking easier. The mechanism for the effect of Ca^{2+} ion on nerve blocking is shown in Figure S7. Hence, we apply DC current with Ca^{2+} ion depletion to block the nerve more easily.

After exploring the effectiveness of the Ca^{2+} ion depletion, we made *in vivo* experiments for blocking the signal propagation along the nerve with ISM-coated flexible electrodes. The experimental setup used for blocking is shown in Figure 1A (top). In blocking experiments, we used an additional electrode and a second signal source for blocking when compared with the stimulation experiments. As in stimulation

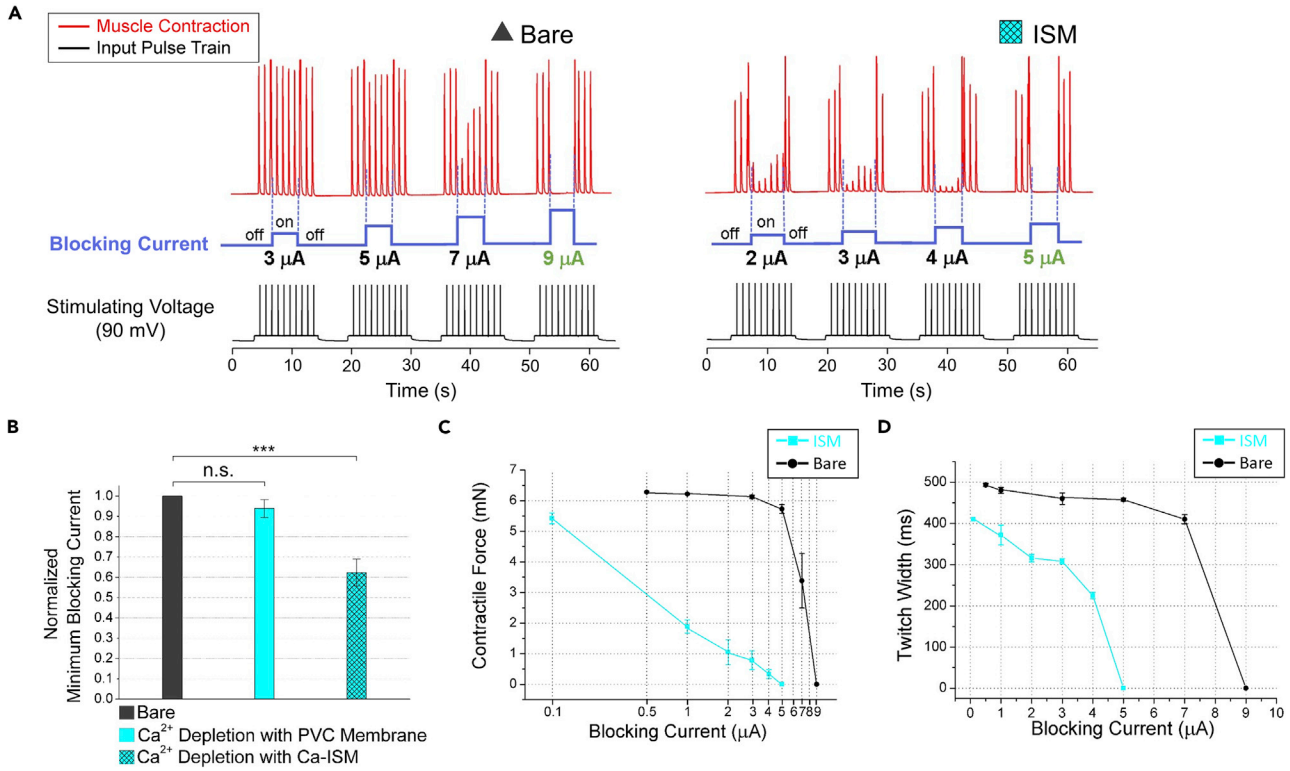

Figure 4. Results of Blocking Experiments with Ca^{2+} Ion Depletion

(A) Blocking experiment results for bare electrode and ISM-coated electrode. The blocking current is applied after the third stimulation pulse for four or five pulse duration. The current needed for full blocking decreases from 9 to 5 μA using ISM-coated electrode.

(B) Comparison of blocking current values for bare electrode, PVC-coated electrode, and ISM-coated electrode (n = 3). The values are normalized with respect to bare electrode. The currents needed to obtain full blocking are very similar for the PVC-coated and the bare electrodes, whereas there is 38% decrease for the ISM-coated electrode. V_s = 90 mV (stimulus), I_b = 1 μA → 100 μA in 1-μA step (DC blocking), t_p = 1 ms (pulse width), f = 1 Hz (pulse frequency), n.s., not significant, ***p < 0.001, error bars represent 2 SD.

(C) Average and standard deviation of contractile force (mN) measured for varying blocking current (μA) in log scale for bare electrode and ISM-coated electrode obtained from the results in (A).

(D) Average and standard deviation of contractile force twitch width (ms) measured for varying blocking current (μA) for the bare electrode and ISM-coated electrode obtained from the results in (A). First large and then small axons are blocked with ISM-coated electrode.

experiments, we first stimulated the sciatic nerve using stimulating electrode by applying pulsed DC current from function generator that contracts the gastrocnemius muscle. Then, we used blocking electrode by applying DC current with source meter. We measured the contractile force from force transducer and monitored it from the PC together with the input signals. Figure 1C (left) illustrates the operating principle of the flexible blocking electrode. We used (+/-/-) configuration for the blocking electrode and coated the ISM on the negatively polarized middle pole. When we apply the DC current, as negatively charged ISM attracts the positively charged Ca^{2+} ions, Ca^{2+} ion concentration around the nerve decreases as schematically shown in Figure 1C (right), which enables us to block the nerve more easily.

In blocking experiments, we first blocked the nerve with bare electrode and then repeated the same procedure with the ISM-coated electrode and compared the results. We applied incrementing input currents to the blocking electrode. We first observed partial blocking and then full blocking because the degree of the nerve blockage depends on the magnitude of current. The experimental results can be seen in Figure 4. Figure 4A presents that the current needed for full blocking decreases from 9 to 5 μA using ISM. We got an average decrease of 38% in full blocking current for three experiments. We obtained full blocking ranging from 5 to 60 μA in sciatic nerve of the frog in our experiments; however, in literature, 0.15–3.0 mA blocking current was used in sciatic nerve of the rat (Vrabec et al., 2015). Also when we turned off the blocking electrode, contractile force returned back to similar values before blocking current application as can be seen from Figure 4A. Therefore we can conclude that we achieved reversible blocking and hence had control on blocking.

We performed a control experiment to prove that the decrement in the blocking current results from the Ca^{2+} ion depletion around the nerve. For this purpose, we used the Ca^{2+} ionophore lacking PVC-coated electrode. As shown in Figure 4B, the current needed for full blocking is very similar in the PVC-coated and the bare electrodes, whereas there is a significant decrease in the ISM-coated electrode. These results show that Ca^{2+} ion depletion around the nerve is responsible in the decrease of blocking current.

Electrical methods cannot be used to block the nerve in chronic clinical applications as they can damage the nerve (Whitwam and Kidd, 1975; Ravid and Prochazka, 2014). EIM uses lower blocking currents, hence does not cause nerve damage. Therefore, EIM has potential to take place in treatment procedure of several disorders caused by uncontrolled neural firing rates, such as chronic pain and epilepsy (Fridman and Della Santina, 2013).

In addition to decreasing the blocking current, we also explored the level of control on blocking using ISM. We studied the relationship between the contractile force of the gastrocnemius muscle and the magnitude of the blocking DC current and obtained the graph shown in Figure 4C. When we use bare electrode, we observe a very sharp decline in the contractile force of the muscle, hence limited control was achieved on partial blockage. However, with ISM-coated electrode, we observe a smooth decline in the contractile force until obtaining full blocking. These results demonstrate that we manage the blocking process in a well-controlled manner with ISM and achieve graded blocking. Graded blocking can be used in peripheral nerves to achieve voluntary movements in hypertonic conditions resulting from stroke (Bhadra and Chae, 2009).

Graded nerve blocking is related to selective blocking of axons. It is known that the velocity of the signal propagation is faster in large axons: the smaller the twitch width, the larger the axons that are activated, and vice versa. Hence, blocking large axons results in small decrease in compound twitch width. As can be seen in Figure 4D, because the large axons get blocked first, we first observe a small decrease from the compound twitch width. However, as we increase the blocking DC current, due to blockage of the small axons, we obtain full blocking. Therefore, we first block large axons and then small axons using ISM. There is, however, a sharp decrease in the twitch width with the bare electrode, because both the large and the small axons in the sciatic nerve are blocked simultaneously. Hence, we achieve selective blocking using ISM-coated electrode.

EIM with Ca^{2+} Ion Enhancement

The stimulation and blockage results given in Figures 2 and 4 show the usage of EIM for *in vivo* and real-time Ca^{2+} ion depletion. Through this modulation, we obtain a more excitable neural membrane environment; hence we increase the V_m of the nerve, which enables us to stimulate and block the signal propagation on the axon more easily in a more controlled way. Taking this control one step further, we aimed to decrease V_m, by creating a more resistant neural membrane environment. For this purpose, we designed a new experiment to increase the Ca^{2+} ion concentration around the sciatic nerve. Figure 5 shows the operating principle and experimental results of EIM for the Ca^{2+} enhancement around the nerve. Figure 5A (left) demonstrates the operating principle of the device for Ca^{2+} enhancement where we coat ISMs on the both sides of the electrode and then load Ca^{2+} ions to ISMs. Ca^{2+} ion loading procedure can be seen in the Transparent Methods section. To measure the stimulation threshold, we placed the sciatic nerve on the bare side of the flexible electrode. Similar to the stimulation experiments with Ca^{2+} ion depletion, we applied the pulsed DC current in (+/-/+) configuration and recorded the stimulation threshold value. For comparison, we placed the nerve on the Ca^{2+}-loaded ISM-coated side of the electrode and repeated the same procedures. Figure 5A (right) demonstrates that positively polarized ISMs repel the positively charged Ca^{2+} ions into the sciatic nerve, thus enhancing the Ca^{2+} ion concentration around the nerve. Figure 5B illustrates that stimulation threshold was increased from 110 to 145 mV by using ISM-coated electrode. We obtained stimulation threshold ranging from 145 to 170 mV with Ca^{2+} enhancement using ISM and obtained an average increase of 45% in the stimulation threshold for three experiments. These results demonstrate that by enhancing Ca^{2+} ion concentration around the nerve, we decrease the V_m, obtain more resistant membrane environment, and increase the stimulation threshold.

To show that the stimulation threshold increment results from the Ca^{2+} ion enhancement around the nerve, we performed control experiments using PVC-coated electrode. PVC-coated electrode is not capable of keeping the Ca^{2+} ions due to absence of the Ca^{2+} ionophore; hence we do not expect Ca^{2+} ion concentration enhancement around the nerve. We stimulated the sciatic nerve and recorded the thresholds

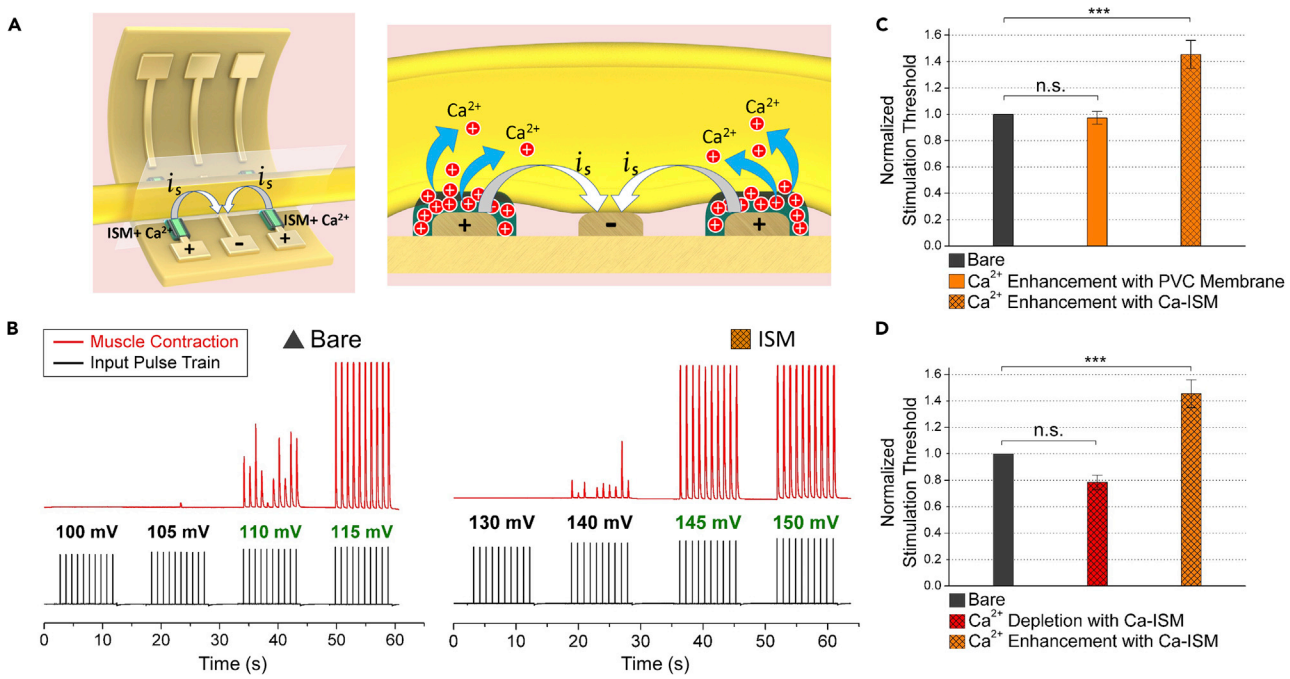

Figure 5. Operating Principle of EIM and Results of Stimulation Experiments with Ca^{2+} Ion Enhancement

(A) Operating principle of EIM with Ca^{2+} ion enhancement. Schematic drawing of the flexible stimulating electrode and the operating principle of the device (left); cross section of sciatic nerve and flexible stimulating electrode to demonstrate the operating principle of ion selective membrane (ISM) (right).

(B) Stimulation experiment results for bare electrode and ISM-coated electrode. Stimulation threshold is increased from 110 to 145 mV by using ISM-coated electrode.

(C) Comparison of stimulation threshold values for bare electrode, PVC-coated electrode, and ISM-coated electrode (n = 3). The values are normalized with respect to bare electrode. The stimulation thresholds are nearly the same for PVC-coated and bare electrodes; however, there is 45% increase for ISM-coated electrode. V_s = 30 mV→230 mV in 5-mV step (stimulus), t_p = 1 ms (pulse width), f = 1 Hz (pulse frequency), n.s., not significant, ***$p < 0.001$, error bars represent 2 SD.

(D) Comparison of stimulation threshold values for bare electrode, ISM-coated electrode with Ca^{2+} ion depletion, and ISM-coated electrode with Ca^{2+} ion enhancement (n = 3). The values are normalized with respect to bare electrode. There is 22% decrease in stimulation threshold using ISM-coated electrode with Ca^{2+} ion depletion and 45% increase using ISM-coated electrode with Ca^{2+} ion enhancement. By depleting or enhancing Ca^{2+} ions around the nerve, we can either decrease or increase stimulation threshold. V_s = 60 mV→170 mV in 2-mV step (stimulus), t_p = 1 ms (pulse width), f = 1 Hz (pulse frequency), n.s., not significant, ***$p < 0.001$, error bars represent 2 SD.

with bare and PVC-coated electrodes. The results shown in the Figure 5C are consistent with our hypothesis: the stimulation thresholds are nearly the same in the PVC-coated and bare electrodes; however, there is an average increase of 45% in the stimulation threshold of ISM-coated electrode. Therefore, increment in stimulation threshold by using ISM-coated electrode results from the Ca^{2+} enhancement around the nerve.

We performed Ca^{2+} imaging experiments as further control experiments to prove Ca^{2+} ion repulsion using ISM. We reversed the polarity of the experiment demonstrated in Figure S4B, where the Ca^{2+} ion bound with Fluo-4 AM dye, and applied 10μA current for 80 s. The positively charged ISM pushes the positively charged Ca^{2+} ions. Therefore, Ca^{2+} ion concentration is decreased. As a result, Fluo-4 AM emission is decreased as shown in Figure S4C. The Fluo-4 AM fluorescence intensity is also decreased as depicted in Figure S4D (right). We also calculated the Ca^{2+} ion concentration decrease using the measured fluorescence intensity. The Ca^{2+} ion concentration decreased from 715 to 37.96 nM after 10 μA current application for 80 s. This experiment demonstrates that we repulsed Ca^{2+} ions using ISM. The Ca^{2+} ion repulsion experiment results are demonstrated in Video S2.

Stimulation experiment results of EIM for Ca^{2+} ion depletion and enhancement are shown in Figure 5D. When we deplete Ca^{2+} ions around the nerve, we increase the V_m and hence decrease the threshold for stimulation. In contrast, when we enhance Ca^{2+} ions around the nerve, we decrease the V_m and therefore increase the threshold for stimulation. Thus we can totally control the V_m with EIM.

		Neuromodulation Methods				
		Electrical	Chemical	Electrochemical	Optogenetics	EIM
Properties	Real time	✓	✗	✗	✓	✓
	Real-life applicability	✓	✓	✗	✗	✓
	Selective stimulation/ blocking of large/small axons	✗	✗	✗	✗	✓
	Stimulation of single neuron	✗	✗	✗	✓	✗
	Latency (delay)	✗	✓	✓	✗	✗
	Side effects	✗	✓	✗	✓	✗
	High-power consumption	✓	✗	✗	✗	✗
	High temporal resolution	✓	✗	✗	✓	✓

Table 1. Properties of Neuromodulation Methods

DISCUSSION

Comparison of EIM with other neuromodulation methods reveals that electrical methods, optogenetics, and EIM have the capability of working in real time, but chemical and electrochemical methods do not have this capability because they work with latency. Electrical methods, chemical methods, and EIM have the potential to be used in real-life applications. However; electrochemical methods work with delay in every single usage; optogenetics genetically alters the neurons and exhibits side effects. Hence, electrochemical methods and optogenetics are not suitable for daily-life applications. Even though chemical methods have the capability of being used in real-life applications, they work with latency and exhibit side effects, which cause termination of the treatment. Electrical methods, optogenetics, and EIM exhibit high temporal resolution. On the other hand, electrical methods cause high power consumption, which is not desirable for the nerve and the patient. EIM is the only method capable of achieving selective stimulation and blocking of large and small axons. Thus, it provides improved stimulation or blocking resolution and more accurate force control. Optogenetics is capable of stimulation of single neuron. By considering all the features mentioned above, it can be said that EIM and optogenetics present the best neuromodulation properties. However, because optogenetics is not suitable for daily-life applications, EIM is superior to optogenetics. Therefore, EIM is the most superior neuromodulation method for real-life applications among all these techniques. Properties of the neuromodulation methods are listed in Table 1.

In addition to the differences demonstrated in Table 1, another fundamental novelty of EIM is its working principle. Electrical methods apply AC and perform just electrical modulation, chemical methods utilize pharmacological agents for chemical modulation, and optogenetics executes chemical modulation via light. Electrochemical methods separate electrical and chemical modulation. These methods apply DC for chemical modulation and AC for electrical modulation. EIM does not separate electrical and chemical modulation. EIM applies pulsed DC and performs electrical and chemical modulation at the same time. In addition to the working principle, EIM also exhibits properties that the other neuromodulation methods do not demonstrate. Electrochemical methods only presented ion concentration depletion. EIM is the only method that demonstrated ion concentration depletion and enhancement around the nerve practically.

In conclusion, we developed a technique, EIM, where we used an interface to both deplete and enhance the Ca^{2+} ion concentration around the sciatic nerve *in vivo* in real time and changed the excitability of the neural membrane environment using flexible electrodes. We achieved better control over V_m compared with electrical stimulation and hence decreased the current needed for stimulating or blocking the nerve. Thus, we obtained more precise force control and better selectivity; thereby EIM could open new avenues in the field of neuromodulation. The discovery of Hodgkin and Huxley (Hodgkin and Huxley, 1952) action potential is a result of the ion concentration change around the nerve and has not been directly applied to daily life due to lack of technology. By utilizing their discovery, EIM has the potential to be a paradigm-shifting method for treatment of neurological disorders. EIM may be used in the development of

neuroprosthetic devices for paralysis (Ho et al., 2014), deep brain stimulation for Parkinson disease (De Hemptinne et al., 2015), stimulating devices for inducing nerve regeneration (van den Brand et al., 2012), and inhibition of nerve activation for migraine (Akerman et al., 2006) and may also play a role in therapy of other neurological disorders. If one achieves the use of EIM in other parts of the nervous system, such as in the brain, holistic control over the motion, sensation, and behavior can be obtained.

Limitations of the Study

In this work, we demonstrated a neuromodulation method, EIM, which is the most superior neuromodulation method for real-life applications. We performed *in vivo* experiments, but we did not observe EIM experiment subjects for months. Future studies should be focused on long-term observations to prepare EIM method for clinical research.

METHODS

All methods can be found in the accompanying Transparent Methods supplemental file.

DATA AND CODE AVAILABILITY

Data generated in this study will be provided upon reasonable request to the lead contact, Rohat Melik (rmelik@etu.edu.tr).

LabVIEW was accessed at http://www.ni.com/sv-se/shop/labview.html (identifier: RRID:SCR_014325); Origin at https://www.originlab.com; and LabScribe at https://www.iworx.com/research/software/labscribe/.

SUPPLEMENTAL INFORMATION

Supplemental Information can be found online at https://doi.org/10.1016/j.isci.2019.06.038.

ACKNOWLEDGMENTS

This work was supported by The Scientific and Technological Research Council of Turkey (TUBITAK) 113S081 grant. We thank to Y. Tatar, A. Şahin, and F. Tokgöz for their help in experiments. We also thank to U. Bağcı for critical reading of the manuscript.

AUTHOR CONTRIBUTIONS

R.M. conceived the idea, designed, and supervised the project. Z.S., S.Ş., B.A., Ç.E., and R.M. designed experiments. Z.S., S.Ş., F.M.B.E., U.Ç.E., E.N.Ş., B.Ş., and M.M. performed experiments. Z.S., S.Ş., and R.M. analyzed data. R.M wrote the manuscript and Z.S, S.Ş, F.M.B.E., U.Ç.E., and Ç.E. contributed to its editing.

DECLARATION OF INTERESTS

R.M. has a pending patent application (TR Patent: 2019/08,576) related to this work. The other authors declare no conflict of interest.

Received: March 18, 2019
Revised: May 11, 2019
Accepted: June 28, 2019
Published: July 26, 2019

REFERENCES

Akerman, S., Holland, P.R., and Goadsby, P.J. (2006). Cannabinoid (CB_1) receptor activation inhibits trigeminovascular neurons. J. Pharmacol. Exp. Ther. *320*, 64–71.

Armstrong, C.M., and Cota, G. (1999). Calcium block of Na^+ channels and its effect on closing rate. Proc. Natl. Acad. Sci. U S A *96*, 4154–4157.

Bhadra, N., and Chae, J. (2009). Implantable neuroprosthetic technology. NeuroRehabilitation *25*, 69–83.

Boger, A.S., Bhadra, N., and Gustafson, K.J. (2012). High frequency sacral root nerve block allows bladder voiding. Neurourol. Urodyn. *31*, 677–682.

Bouton, C.E., Shaikhouni, A., Annetta, N.V., Bockbrader, M.A., Friedenberg, D.A., Nielson, D.M., Sharma, G., Sederberg, P.B., Glenn, B.C., Mysiw, W.J., et al. (2016). Restoring cortical control of functional movement in a human with quadriplegia. Nature *533*, 247–250.

Boyden, E.S., Zhang, F., Bamberg, E., Nagel, G., and Deisseroth, K. (2005). Millisecond-timescale, genetically targeted optical control of neural activity. Nat. Neurosci. *8*, 1263–1268.

van den Brand, R., Heutschi, J., Barraud, Q., DiGiovanna, J., Bartholdi, K., Huerlimann, M., Friedli, L., Vollenweider, I., Moraud, E.M., Duis, S., et al. (2012). Restoring voluntary control of locomotion after paralyzing spinal cord injury. Science *336*, 1182–1185.

Butler, A.B., and Hodos, W. (2005). Comparative Vertebrate Neuroanatomy: Evolution and Adaptation, Second Edition (John Wiley & Sons).

Campbell, N.A., Reece, J.B., Urry, L.A., Cain, M.L., Wasserman, S.A., Minorsky, P.V., and Jackson, R.B. (2015). Biology A Global Approach, Tenth Edition (Essex: Pearson Education Limited).

Choi, C.Y. (2016). Chronic pain and opiate management. Dis. Mon. *62*, 334–345.

Elefteriades, J.A., Quin, J.A., Hogan, J.F., Holcomb, W.G., Letsou, G.V., Chlosta, W.F., and Glenn, W.W. (2002). Long-term follow-up of pacing of the conditioned diaphragm in quadriplegia. Pacing Clin. Electrophysiol. *25*, 897–906.

Foutz, T.J., Ackermann, D.M., Jr., Kilgore, K.L., and McIntyre, C.C. (2012). Energy efficient neural stimulation: coupling circuit design and membrane biophysics. PLoS One *7*, e51901.

Fridman, G.Y., and Della Santina, C.C. (2013). Safe direct current stimulation to expand capabilities of neural prostheses. IEEE Trans. Neural Syst. Rehabil. Eng. *21*, 319–328.

Gao, W., Emaminejad, S., Nyein, H.Y.Y., Challa, S., Chen, K., Peck, A., Fahad, H.M., Ota, H., Shiraki, H., Kiriya, D., et al. (2016). Fully integrated wearable sensor arrays for multiplexed in situ perspiration analysis. Nature *529*, 509–514.

Gilron, I., Baron, R., and Jensen, T. (2015). Neuropathic pain: principles of diagnosis and treatment. Mayo Clin. Proc. *90*, 532–545.

Harris, J.D. (2008). Management of expected and unexpected opioid-related side effects. Clin. J. Pain. *24*, S8–S13.

De Hemptinne, C., Swann, N.C., Ostrem, J.L., Ryapolova-Webb, E.S., San Luciano, M., Galifianakis, N.B., and Starr, P.A. (2015). Therapeutic deep brain stimulation reduces cortical phase-amplitude coupling in Parkinson's disease. Nat. Neurosci. *18*, 779–786.

Ho, C.H., Triolo, R.J., Elias, A.L., Kilgore, K.L., DiMarco, A.F., Bogie, K., Vette, A.H., Audu, M.L., Kobetic, R., Chang, S.R., et al. (2014). Functional electrical stimulation and spinal cord injury. Phys. Med. Rehabil. Clin. N. Am. *25*, 631–654.

Hochberg, L.R., Bacher, D., Jarosiewicz, B., Masse, N.Y., Simeral, J.D., Vogel, J., Haddadin, S., Liu, J., Cash, S.S., van der Smagt, P., et al. (2012). Reach and grasp by people with tetraplegia using a neurally controlled robotic arm. Nature *485*, 372–375.

Hodgkin, A.L., and Huxley, A.F.A. (1952). Quantitative description of membrane current and its application to conduction and excitation in nerve. J. Physiol. *117*, 500–544.

Kandel, E.R., Schwartz, J.H., Jessell, T.M., Siegelbaum, S.A., and Hudspeth, A.J. (2013). Principles of Neural Science, Fifth Edition (McGraw-Hill).

Kang, T.M., and Hilgemann, D.W. (2004). Multiple transport modes of the cardiac Na^{+}/Ca^{2+} exchanger. Nature *427*, 544–548.

Luan, S., Williams, I., Nikolic, K., and Constandinou, T.G. (2014). Neuromodulation: present and emerging methods. Front. Neuroeng. *7*, 27.

Mazurek, K.A., Holinski, B.J., Everaert, D.G., Stein, R.B., Etienne-Cummings, R., and Mushahwar, V.K. (2012). Feed forward and feedback control for over-ground locomotion in anaesthetized cats. J. Neural Eng. *9*, 026003.

Melo, P.L., Silva, M.T., Martins, J.M., and Newman, D.J. (2015). Technical developments of functional electrical stimulation to correct drop foot: sensing, actuation and control strategies. Clin. Biomech. *30*, 101–113.

Memberg, W.D., Polasek, K.H., Hart, R.L., Bryden, A.M., Kilgore, K.L., Nemunaitis, G.A., Hoyen, H.A., Keith, M.W., and Kirsch, R.F. (2014). Implanted neuroprosthesis for restoring arm and hand function in people with high level tetraplegia. Arch. Phys. Med. Rehabil. *95*, 1201–1211.e1.

Micera, S., Keller, T., Lawrence, M., Morari, M., and Popovic, D.B. (2010). Wearable neural prostheses. IEEE Eng. Med. Biol. *29*, 64–69.

Nataraj, R., Audu, M.L., and Triolo, R.J. (2012). Comparing joint kinematics and center of mass acceleration as feedback for control of standing balance by functional neuromuscular stimulation. J. Neuroeng. Rehabil. *9*, 25.

Onders, R.P., DiMarco, A.F., Ignagni, A.R., Aiyar, H., and Mortimer, J.T. (2004). Mapping the phrenic nerve motor point: the key to a successful laparoscopic diaphragm pacing system in the first human series. Surgery *136*, 819–826.

Peckham, P.H., and Kilgore, K.L. (2013). Challenges and opportunities in restoring function after paralysis. IEEE Trans. Biomed. Eng. *60*, 602–609.

Peckham, P.H., and Knutson, J.S. (2005). Functional electrical stimulation for neuromuscular applications. Annu. Rev. Biomed. Eng. *7*, 327–360.

Plesha, M.A., Van Wie, B.J., Mullin, J.M., and Kidwell, D.A. (2006). Measuring quaternary ammonium cleaning agents with ion selective electrodes. Anal. Chim. Acta *570*, 186–194.

Ravid, E., and Prochazka, A. (2014). Controlled nerve ablation with direct current: parameters and mechanisms. IEEE Trans. Neural Syst. Rehabil. Eng. *22*, 1172–1185.

Ridge, R.M.A.P. (1967). The differentiation of conduction velocities of slow twitch and fast twitch muscle motor innervations in kittens and cats. Q. J. Exp. Physiol. Cogn. Med. Sci. *52*, 293–304.

Rohde, L.M., Bonder, B.R., and Triolo, R.J. (2012). Exploratory study of perceived quality of life with implanted standing neuroprostheses. J. Rehabil. Res. Dev. *49*, 265–278.

Sadowsky, C.L., Hammond, E.R., Strohl, A.B., Commean, P.K., Eby, S.A., Damiano, D.L., Wingert, J.R., Bae, K.T., and McDonald, J.W. (2013). Lower extremity functional electrical stimulation cycling promotes physical and functional recovery in chronic spinal cord injury. J. Spinal Cord Med. *36*, 623–631.

Solis, L.R., Gyawali, S., Seres, P., Curtis, C.A., Chong, S.L., Thompson, R.B., and Mushahwar, V.K. (2011). Effects of intermittent electrical stimulation on superficial pressure, tissue oxygenation, and discomfort levels for the prevention of deep tissue injury. Ann. Biomed. Eng. *39*, 649–663.

Solis, L.R., Liggins, A., Uwiera, R.R.E., Poppe, N., Pehowich, E., Seres, P., Thompson, R.B., and Mushahwar, V.K. (2012). Distribution of internal pressure around bony prominences: implications to deep tissue injury and effectiveness of intermittent electrical stimulation. Ann. Biomed. Eng. *40*, 1740–1759.

Song, Y.A., Melik, R., Rabie, A.N., Ibrahim, A.M.S., Moses, D., Tan, A., Han, J., and Lin, S.J. (2011). Electrochemical activation and inhibition of neuromuscular systems through modulation of ion concentrations with ion-selective membranes. Nat. Mater. *10*, 980–986.

Theogarajan, L. (2012). Strategies for restoring vision to the blind: current and emerging technologies. Neurosci. Lett. *519*, 129–133.

Triolo, R.J., Bailey, S.N., Miller, M.E., Rohde, L.M., Anderson, J.S., Davis, J.A., Jr., Abbas, J.J., DiPonio, L.A., Forrest, G.P., Gater, D.R., Jr., et al. (2012). Longitudinal performance of a surgically implanted neuroprosthesis for lower-extremity exercise, standing, and transfers after spinal cord injury. Arch. Phys. Med. Rehabil. *93*, 896–904.

Triolo, R.J., Bailey, S.N., Miller, M.E., Lombardo, L.M., and Audu, M.L. (2013a). Effects of stimulating hip and trunk muscles on seated stability, posture, and reach after spinal cord injury. Arch. Phys. Med. Rehabil. *94*, 1766–1775.

Triolo, R.J., Bailey, S.N., Lombardo, L.M., Miller, M.E., Foglyano, K., and Audu, M.L. (2013b). Effects of intramuscular trunk stimulation on manual wheelchair propulsion mechanics in 6 subjects with spinal cord injury. Arch. Phys. Med. Rehabil. *94*, 1997–2005.

Vrabec, T., Bhadra, N., Wainright, J., Bhadra, N., Franke, M., and Kilgore, K. (2015). Characterization of high capacitance electrodes for the application of direct current electrical nerve block. Med. Biol. Eng. Comput. *54*, 191–203.

Wang, E., Erdahl, W.L., Hamidinia, S.A., Chapman, C.J., Taylor, R.W., and Pfeiffer, D.R. (2001). Transport properties of the calcium ionophore ETH-129. Biophys. J. *81*, 3275–3284.

Weiss, T.F. (1996). Cellular Biophysics: Electrical Properties, *Vol. 2* (MIT press).

Wenger, N., Moraud, E.M., Gandar, J., Musienko, P., Capogrosso, M., Baud, L., Le Goff, C.G., Barraud, Q., Pavlova, N., Dominici, N., et al. (2016). Spatiotemporal neuromodulation therapies engaging muscle synergies improve motor control after spinal cord injury. Nat. Med. *22*, 138–145.

Whitwam, J.G., and Kidd, C. (1975). The use of direct current to cause selective block of large fibres in peripheral nerves. Br. J. Anaesth. *47*, 1123–1132.

Wu, G.A., Lombardo, L., Triolo, R.J., and Bogie, K.M. (2013). The effects of combined trunk and gluteal neuromuscular electrical stimulation on posture and tissue health in spinal cord injury. PM R *5*, 688–696.

ISCI, Volume *17*

Supplemental Information

Real-Time *In Vivo* Control of Neural Membrane Potential by Electro-Ionic Modulation

Zafer Soybaş, Sefa Şimşek, F.M. Betül Erol, U. Çiya Erdoğan, Esra N. Şimşek, Büşra Şahin, Merve Marçalı, Bahattin Aydoğdu, Çağlar Elbüken, and Rohat Melik

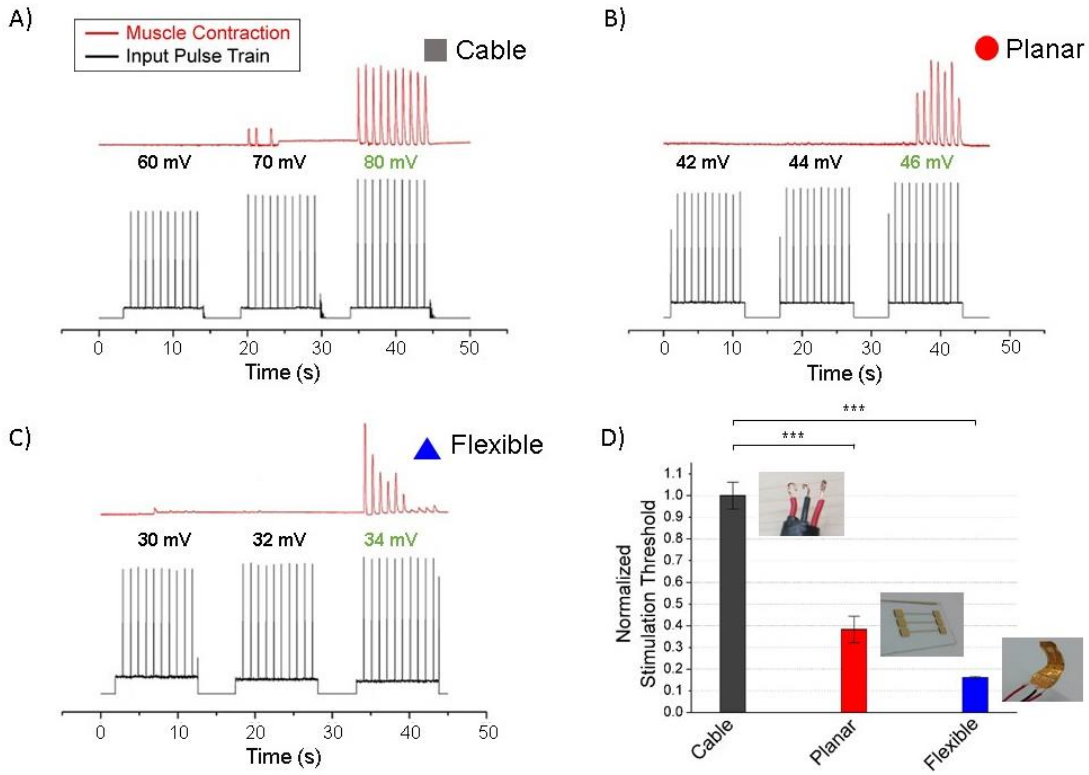

Figure S1. Related to Figure 1. Stimulation experiments with conventional cable, planar electrode and flexible electrode

Stimulation experiment results for (A) conventional cable with 80 mV threshold, (B) planar electrode with 46 mV threshold, (C) flexible electrode with 34 mV threshold. (D) Comparison of stimulation threshold values for conventional cable, planar electrode and flexible electrode (n=3). The values are normalized with respect to conventional cable. V_s = 25 mV→240 mV in 2 mV step (stimulus), t_p = 1 ms (pulse width), f = 1 Hz (pulse frequency), ***p<0.001, error bars represent 2 s.d.

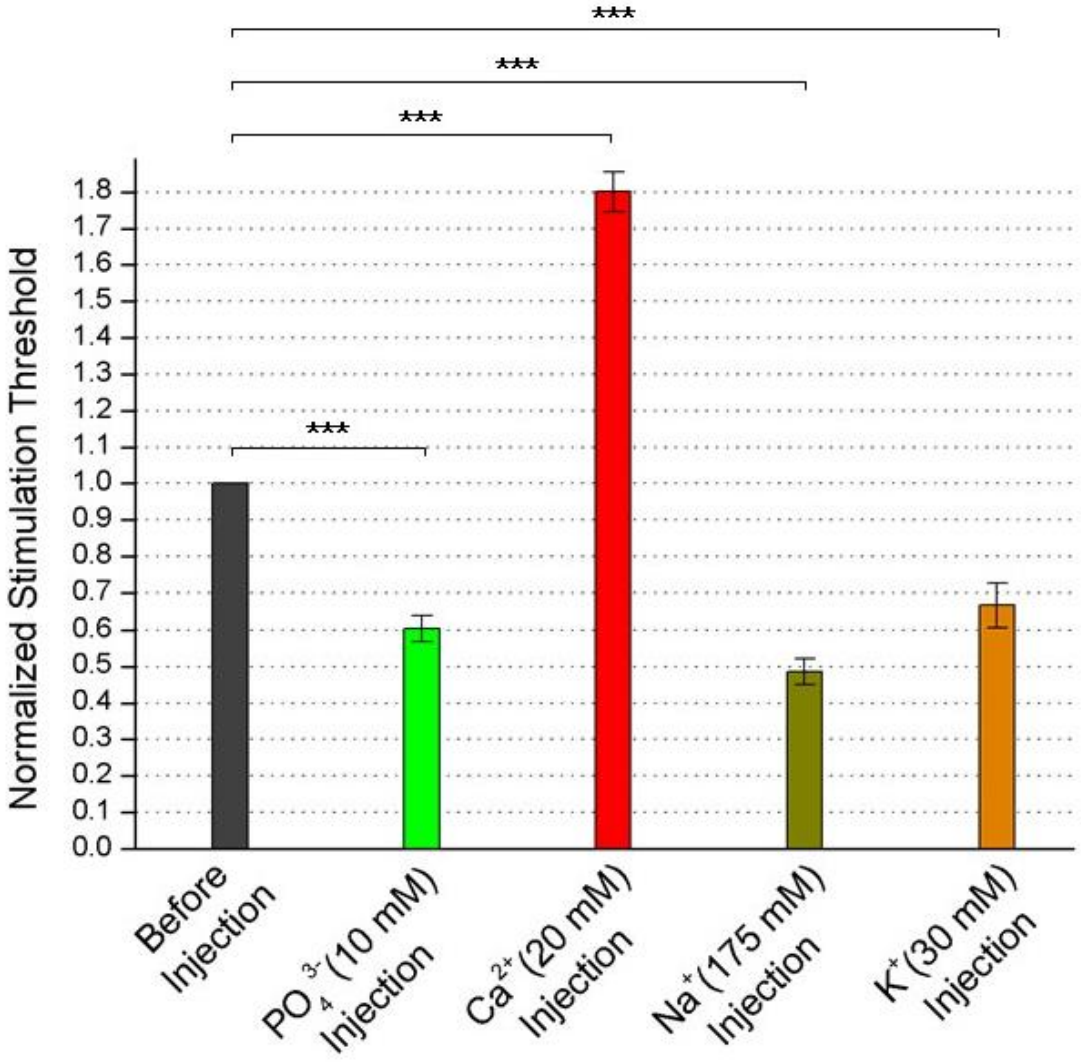

Figure S2. Related to Figure 2. Stimulation experiments with *in-vivo* manual ion injections

Comparison of stimulation threshold values for 10 mM PO_4^{3-}, 20 mM Ca^{2+}, 175 mM Na^+, and 30 mM K^+ manual ion injections into the sciatic nerve (n=3). We used PO_4^{3-} ion in order to observe the effect of the Ca^{2+} ion depletion. The values are normalized with respect to before ion injection case. V_s = 16 mV→190 mV in 2 mV step (stimulus), t_p = 1 ms (pulse width), f = 1 Hz (pulse frequency), ***p<0.001, error bars represent 2 s.d.

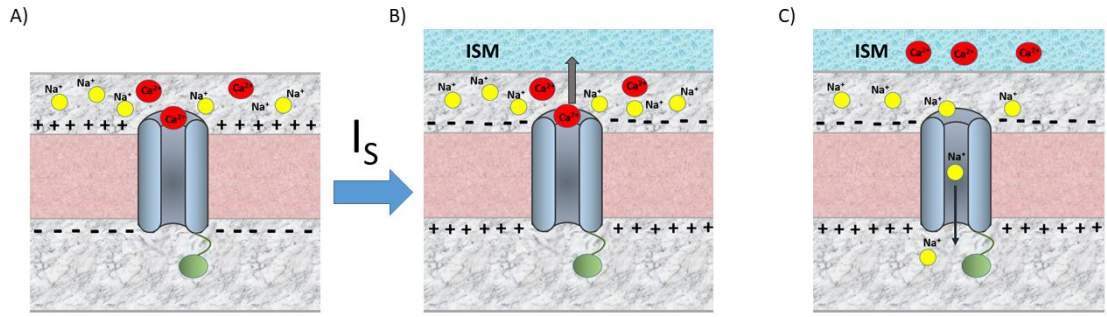

Figure S3. Related to Figure 2. The mechanism for the effect of Ca^{2+} ion on nerve stimulation

(A) Ca^{2+} ion closes the voltage-gated Na^+ channel (Armstrong and Cota, 1999). (B) When we apply stimulation current using ISM, we deplete Ca^{2+} ions around the nerve, (C) the voltage-gated Na^+ channel is opened and Na^+ ions enter voltage-gated Na^+ channel (Kandel et al., 2013).

A)

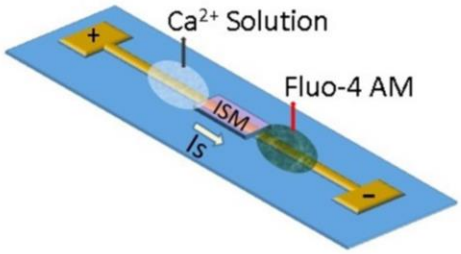
Ca2+ Solution
Fluo-4 AM
ISM
IS
+
-

B)

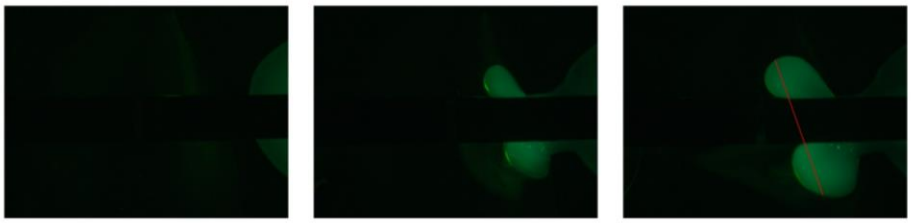

C)

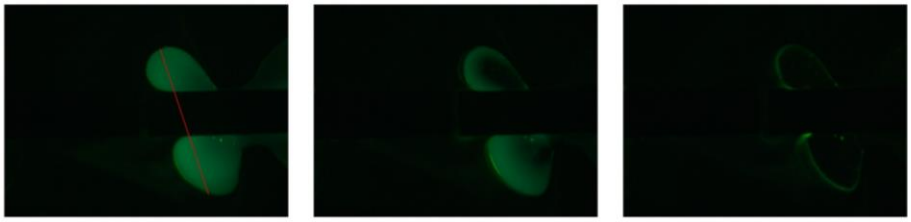

D)

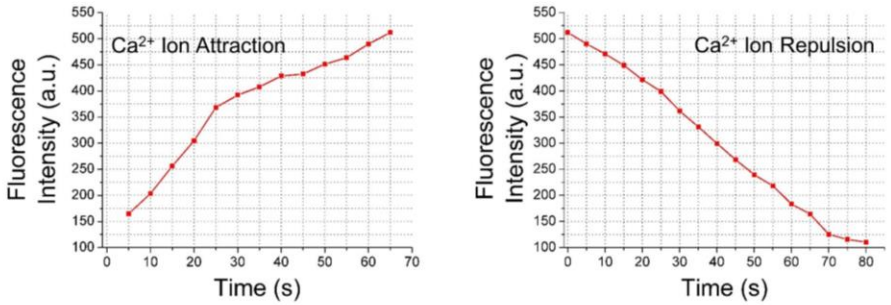
Ca2+ Ion Attraction
Fluorescence Intensity (a.u.)
Time (s)
Ca2+ Ion Repulsion
Fluorescence Intensity (a.u.)
Time (s)

E)

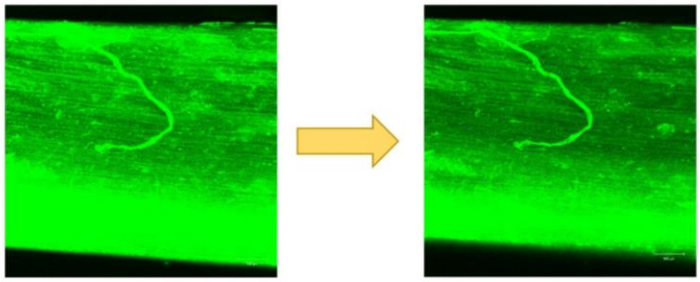

Figure S4. Related to Figure 2. The control experiments for Ca^{2+} ion modulation using ISM

(A) The schematic diagram of our experimental setup for Ca^{2+} imaging for Ca^{2+} ion attraction. (B) Ca^{2+} imaging for Ca^{2+} ion attraction. The left picture is before current application, the middle picture is after 10 μA current application for 30 seconds, the right picture is after 10 μA current application for 65 seconds. Ca^{2+} ions are attracted with current application. The red line is drawn in the right picture to indicate the fluorescence intensity calculation area, which is applied to all the pictures of Ca^{2+} ion attraction experiment. (C) Ca^{2+} imaging for Ca^{2+} ion repulsion. The left picture is before current application, the middle picture is after 10 μA current application for 45 seconds, the right picture is after 10 μA current application for 80 seconds. Ca^{2+} ions are repulsed with current application. The red line is drawn in the left picture to indicate the fluorescence intensity calculation area, which is applied to all the pictures of Ca^{2+} ion repulsion experiment. (D) Fluorescence intensity change in time for Ca^{2+} imaging. The left graph is for Ca^{2+} ion attraction, the right graph is for Ca^{2+} ion repulsion. (E) Confocal imaging of the sciatic nerve of a frog. The left image is before current application and the right image is after 20μA current application for 1 minute. The fluorescence intensity of the Fluo-4 AM (Ca^{2+} Reporter Dye) in the sciatic nerve is decreased after current application. Therefore, Ca^{2+} ions are depleted from sciatic nerve.

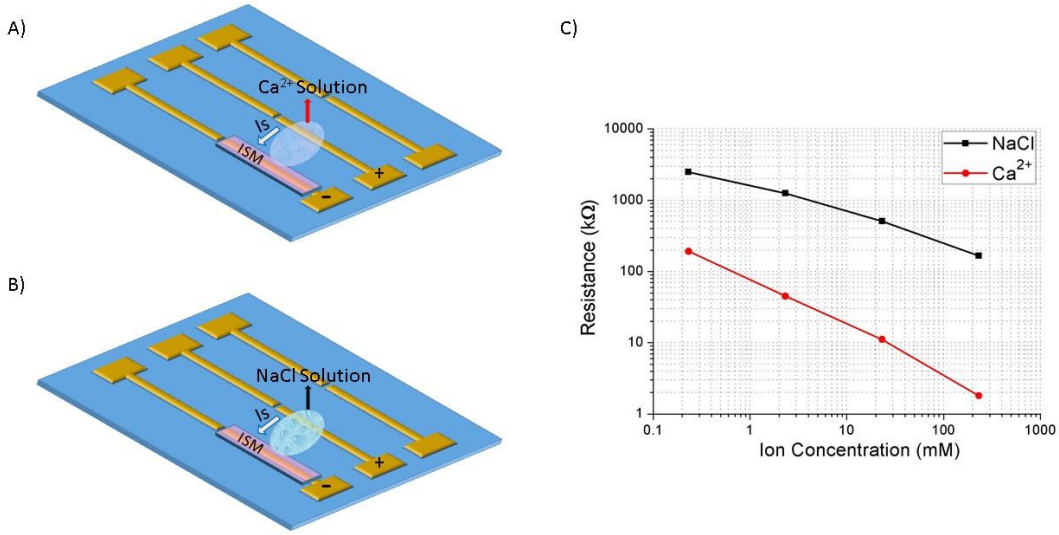

Figure S5. Related to Figure 2. The Ca^{2+} ion selectivity of our device
(A) The schematic diagram of our experimental setup to test the Ca^{2+} ion selectivity of our device using different concentrations of Ca^{2+} solution. (B) The schematic diagram of our experimental setup with different concentrations of NaCl solution. (C) Resistance measurements with different concentrations of Ca^{2+} and NaCl solutions. 232mM, 23.2mM, 2.32mM, 0.232mM Ca^{2+} and NaCl solutions are used in the amount of 4 µL (X and Y axes are in log scale).

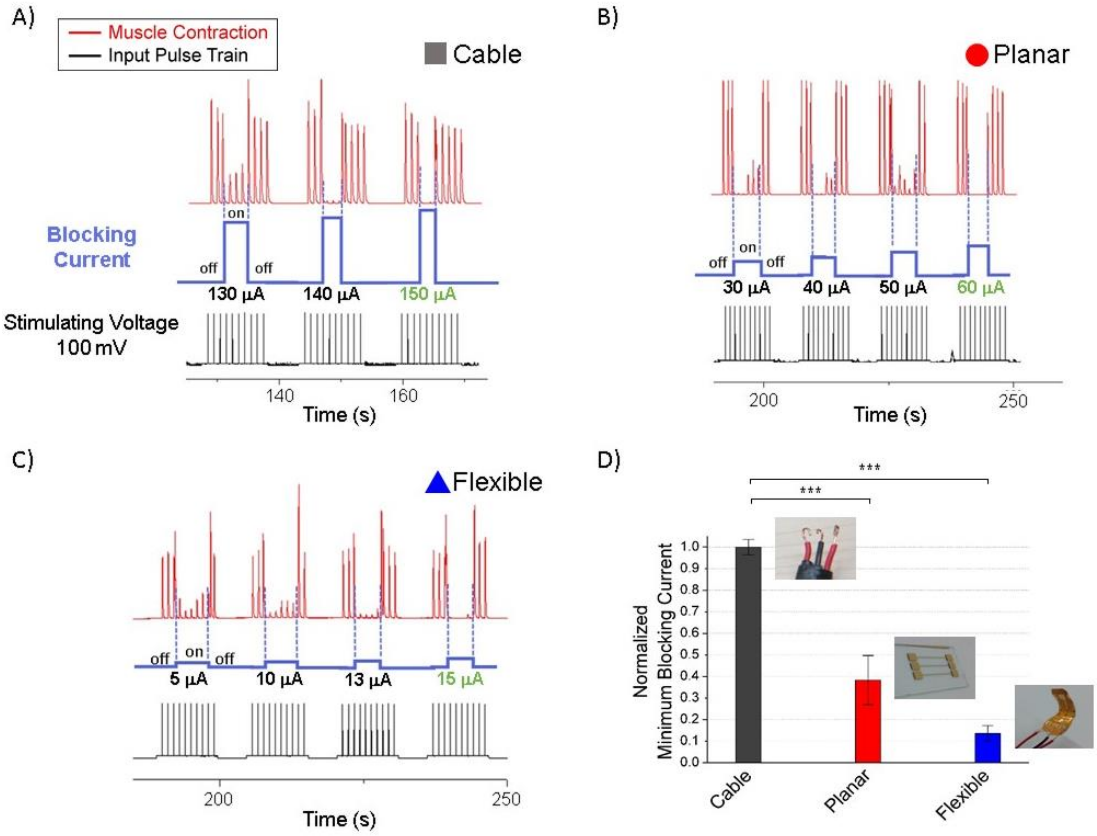

Figure S6. Related to Figure 1. Blocking experiments with conventional cable, planar electrode and flexible electrode

Blocking experiment results for (A) conventional cable with 150 μA full blocking current, (B) planar electrode with 60 μA full blocking current, (C) flexible electrode with 15 μA full blocking current. (D) Comparison of blocking current values for conventional cable, planar electrode and flexible electrode (n=3). The values are normalized with respect to conventional cable. V_s = 100 mV (stimulus), I_b = 1 μA → 100 μA in 0.1 μA step (DC blocking), t_p = 1 ms (pulse width), f = 1 Hz (pulse frequency), ***p<0.001, error bars represent 2 s.d.

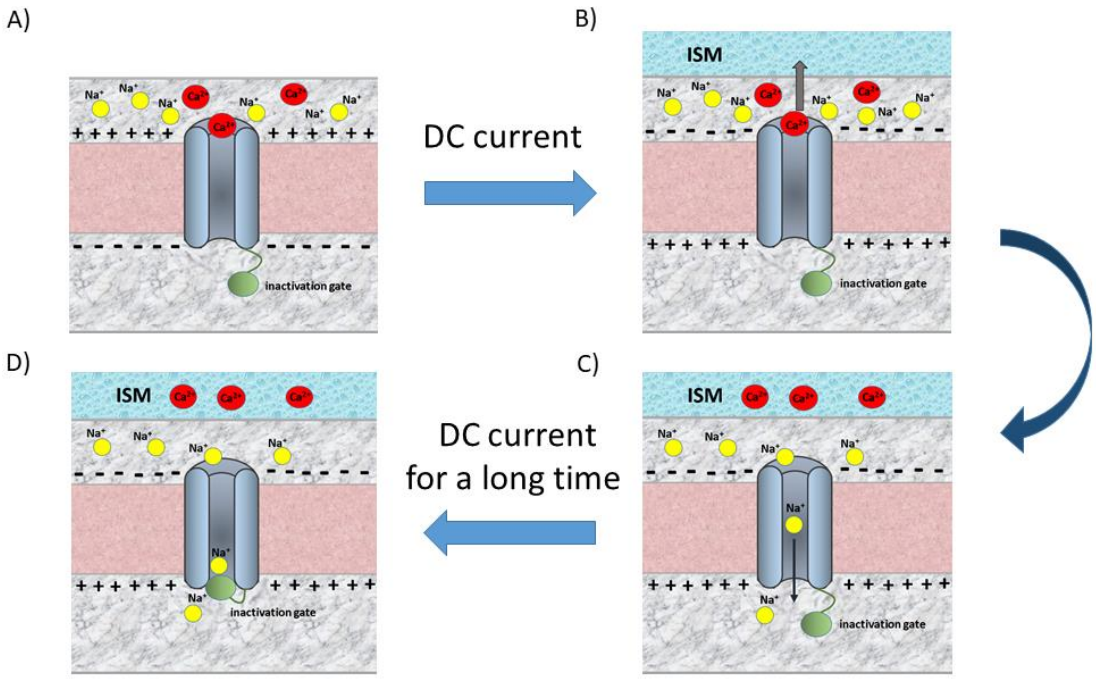

Figure S7. Related to Figure 4. The mechanism for the effect of Ca^{2+} ion on nerve blocking

(A) Ca^{2+} ions prevent Na^{+} ion passage by blocking voltage-gated Na^{+} channels (Armstrong and Cota, 1999). (B) When we apply DC current using ISM, we deplete the Ca^{2+} ions around the nerve, (C) which lets Na^{+} ions to pass more easily through the channel (Kandel et al., 2013). (D) When we apply prolonged DC current, inactivation gate is closed that leads to blockage of Na^{+} transportation and signal propagation along the axon (Kandel et al., 2013).

Transparent Methods

1. Animals

Adult male frogs (*Rana Ridibunda*) weighing between 100-150 grams were acquired for *in-vivo* experiments. 73 sciatic nerves were used for the experiments. Since we used the same sciatic nerve for a single experimental set to compare different cases, we dealt with relative values. Therefore, sex of the subjects does not have any influence on our experiment results. All experimental procedures were performed according to the protocol approved by Dicle University Health Sciences Research and Application Centre (DUSAM) (2016/23).

2. Surgical preparation

The anesthetizing solution was prepared by mixing 0.3-0.5 mL of ketamine (Ketalar®) and 0.4-0.6 mL of serum physiologic isotonic solution. Each frog was sedated with varying doses of ketamine, proportional to its size, injected into its thigh muscles for about 30-60 minutes. Thereafter, dissection procedure was applied on the contralateral leg. Firstly, the skin of leg was totally removed. Then, the sciatic nerve was found and liberated from the surrounding tissues so that the flexible electrode can be placed underneath it. Thereafter, distal part of the gastrocnemius muscle was dissected and a ligature around the Achilles tendon was tied in order to measure the contractile force. This protocol was approved by Dicle University Health Sciences Research and Application Centre (DUSAM) (2016/23).

3. Fabrication of electrode

The electrodes were fabricated through standard lithography techniques and thermal evaporation steps. Briefly, the electrode was patterned by photolithography with positive photoresist (MicroChemicals AZ5214E) on a substrate. We taped kapton tape, which has high temperature resistance as a substrate (Melik et al., 2009), on glass slide. 15 nm Cr / 185 nm Au was deposited on kapton tape via thermal evaporation and lifted-off in acetone. The kapton tape was removed from the glass after lift-off.

4. Preparation of ion selective membranes

Preparation of ion selective membrane was described in many studies (Guenat et al., 2005; Guenat et al., 2006). We optimized the component ratios to obtain maximum performance for our usage. Ion selective membrane was produced by dissolving ion selective cocktail in cyclohexanone. The ion selective membrane cocktail was prepared with the following components: 15.1 wt.% ionophore (ETH 129 for Ca^{2+}), 15.3 wt.% sodium tetraphenylborate, 58.7 wt.% 2-nitrophenyl octyl ether, 10.9 wt.% poly(vinyl chloride) high molecular weight (all Selectophore, Fluka Sigma Aldrich). The ion selective cocktail (333 mg) was dissolved in 0.4 ml cyclohexanone. Then ion selective membrane was coated on previously fabricated electrodes.

5. Fabrication of polydimethyl siloxane (PDMS) channel

We used PDMS microchannels with a depth of 100 µm, a thickness of 1 mm and a length of 9 mm. The mold was fabricated on a 4 inch silicon wafer. First, SU-8 2005 was coated followed by spin coating of SU-8 2050 to a thickness of 50 µm. Subsequently, the wafer is exposed to ultraviolet light. After development in acetone, the mold was obtained. For obtaining the channel, PDMS was mixed at a ratio of 10:1 base polymer and curing agent, well mixed, degassed and poured onto the mold. After curing at 70^{o}C overnight, the microchannel was obtained. The PDMS channels were placed on the electrode under a microscope for selective coating of ISM on the electrodes and seals itself with the weight of the channel. ISM cocktail was injected into the channel manually using a syringe. The thickness of the ISM layer is 100 µm.

6. Manual ion injections

We injected PO_4^{3-} ion in order to observe the effect of the Ca^{2+} ion depletion, as it precipitates the Ca^{2+} ions (Lodish et al., 2003) and decreases the free Ca^{2+} ion concentration without changing the Na^{+} and K^{+} concentration in the environment. Since there is no known compound that selectively precipitates Na^{+} or K^{+} ions (Lodish et al., 2003), we could not observe the effect of depletion of these ions. We adjusted the ion concentrations based on the reported literature (Patnaik, 2004) and optimizations in our experiments with frogs.

7. Confocal Imaging

The confocal images for the proof of the depletion of the Ca^{2+} ions from the nerve using ISM were taken with Zeiss confocal microscope (LSM 710) from the sciatic nerve of a frog. We dissected the sciatic nerve for these experiments and washed the nerve for two hours in Fluo-4 AM dye solution (Ca^{2+} Reporter Dye) before the observation in confocal microscope. To prepare the solution, we dissolved 50 µg Fluo-4 AM in 30 µL methanol and added 500 µL Ringer's solution to this mixture. By this way, we obtained the stock solution. Afterwards, we added 465 µL Ringer's solution to 35µL of the stock solution and obtained 500 µL Fluo-4 AM dye solution, which has 6 µM Fluo-4 AM concentration. We coated the middle-leg of the ITO electrode with ISM for the experiments. Subsequently, we put the sciatic nerve, washed in Fluo-4 AM dye solution, over the electrodes. We placed the electrodes to confocal microscope and applied 20 µA current for 1 minute with (+ - +) polarity order. We observed the fluorescence intensity of the Fluo-4 AM dye solution (Ca^{2+} Reporter Dye) in the sciatic nerve.

8. Ca^{2+} Imaging

We used Zeiss Axio Vert.A1 inverted fluorescence microscope for Ca^{2+} imaging experiments. We used planar electrodes with glass substrate for Ca^{2+} ion attraction and repulsion experiments. For Ca^{2+} ion attraction experiments, we coated ISM on the opposed tips of anode and cathode of the electrode. We applied 2 µL Fluo-4 AM stock solution (which is used in confocal imaging experiments) next to the ISM layer on cathode. We also applied 1 µL of 232mM Ca^{2+} solution next to the ISM layer on anode. Afterwards, we applied 10 µA current for 65 seconds to the Ca^{2+} loaded anode and observed increase in Fluo-4 AM emission on cathode. Subsequently, we made Ca^{2+} ion repulsion experiments. We reversed the polarity of the current application for the same electrode loaded with Ca^{2+} ions in Ca^{2+} ion attraction experiments. We applied 10 µA for 80 seconds and observed decrease in Fluo-4 AM emission.

We used the formula below to calculate Ca^{2+} ion concentration (Non-ratiometric methods):

$$[Ca^{2+}] = K_d \cdot (F - F_{min})/(F_{max}-F)$$

The variables of the formula are:
K_d: The dissociation constant.
F: The observed fluorescence of our sample.
F_{min}: The lowest fluorescent value at fixed experimental conditions.
F_{max}: The highest fluorescent value at the same experimental conditions.

We used K_d as 335 nM (Fluo-4, AM, cell permeant).

9. Ca^{2+} Ion Selectivity Test

The cathode of the planar electrode with glass substrate is coated with ISM as demonstrated in Figure S5A. The anode is covered by Ca^{2+} solution. Ca^{2+} solution touches the ISM between the anode and cathode and completes the circuit. Therefore, when the current is applied the Ca^{2+} ions goes from anode to cathode and accumulate in ISM. The resistance of our experimental setup is measured with different concentrations of Ca^{2+} solution. The same experiment is also performed with the experimental setup presented in Figure S5B, this time we used different concentrations of NaCl solution instead of using different concentrations of Ca^{2+} solution. The resistance of our experimental setup is measured with different concentrations of NaCl solution.

10. Ca^{2+} ion loading

We put commercially available Ca^{2+} solution (232 mM Ca^{2+} solution) against the ISMs on the opposite electrode in Figure 5A. Then, we polarize ISM-coated poles as negative, and Ca^{2+} solution-coated poles as positive and apply 1 µA current for three minutes. Negatively polarized ISMs attract the Ca^{2+} ions from the Ca^{2+} solution so that Ca^{2+} ions are loaded into the ISMs. Then, we clean the Ca^{2+} solutions and perform the *in-vivo* experiments.

References

Armstrong, C.M., and Cota, G. (1999). Calcium block of Na^+ channels and its effect on closing rate. Proc. Natl. Acad. Sci. USA *96*, 4154-4157.

Kandel, E.R., Schwartz, J.H., Jessell, T.M., Siegelbaum, S.A., and Hudspeth, A.J. (2013). Principles of Neural Science (New York: McGraw-Hill). 5th Ed.

Melik, R., Unal, E., Perkgoz, N.K., Puttlitz, C., and Demir, H.V. (2009). Flexible metamaterials for wireless strain sensing. Appl. Phys. Lett. *95*, 181105.

Guenat, O.T., Dufour, J.F., van der Wal, P.D., Morf, W.E., de Rooij, N.F., and Koudelka-Hep, M. (2005). Microfabrication and characterization of an ion-selective microelectrode array platform. Sens. Actuators B Chem. *105*, 65-73.

Guenat, O.T., Generelli, S., de Rooij, N.F., Koudelka-Hep, M., Berthiaume, F., & Yarmush, M.L. (2006). Development of an Array of Ion-Selective Microelectrodes Aimed for the Monitoring of Extracellular Ionic Activities. Anal. Chem*. 78*, 7453-7460.

Lodish, H., Berk, A., Matsudaira, P., Kaiser, C.A., Krieger, M., Scott, M.P., Zipursky, L., and Darnell, J. (2003). Molecular Cell Biology (Freeman, W. H. & Company). 5th Ed.

Patnaik, P. (2004). Dean's Analytical Chemistry Handbook (McGraw-Hill Handbooks). 2nd Ed.

Non-ratiometric methods. (n.d.). Retrieved from https://www.embl.de/eamnet/html/calcium/nonratio.htm

Fluo-4, AM, cell permeant. (n.d.). Retrieved from https://www.thermofisher.com/order/catalog/product/F14201?SID=srch-srp-F14201